



Transmission line fault classification based on spatiotemporal characteristic analysis with global and local discriminant analysis

Tong Zhang^{a,*}, Nan Wang^{b,*}

^a Shenyang Key Laboratory of Information Perception and Edge Computing, School of Artificial Intelligence, Shenyang University of Technology, Shenyang 110000, China

^b College of Mechanical Engineering, Shenyang University, Shenyang 110000, China



ARTICLE INFO

Keywords:

Single line to ground fault classification
Spatiotemporal characteristic analysis
Characteristic entropy
Global and local discriminant analysis
Phasor measurement unit

ABSTRACT

To ensure the reliability of power supply, ultra-fast and reliable fault classification of the transmission line is the critical stage of the wide-area transmission network protection. As the distributed generation (DG) current injection to the transmission line, the amplitude characteristic of the break current protection reduces and the system reliability decreases. With the wide-area measurement generated to the power system, an online fault classification method with the global and local discriminant analysis (GLDA) is proposed to enhance the phase characteristic and decrease calculation load. In the single line to ground (SLG) fault process, the local current phase shift is analyzed to enhance the spatiotemporal characteristic. To fully measure the ordering degree of the spatiotemporal characteristic, the axiomatic definition for the characteristic entropy (CE) of the grid impedance in the individual bus in the wide-area transmission network is proposed according to the characteristic distribution. Based on the current spatiotemporal characteristic analysis, a multi-priority GLDA classifies the fault phase in a coordinating way using with the phasor measurement unit (PMU). The multi-priority GLDA-CE fault classification method reduces the computational load, ensures resilience against measurement noise and the transition resistance effect. Compared with the statistical entropy and neural network method, the classification accuracy and response speed of the GLDA-CE fault classification method are validated in the IEEE 39-bus system with 10 PMUs. Compared with the conventional statistical entropy and neural network methods, the GLDA-CE method is able to classify 226 entire power outages and 600 single phase outages within 1.621 s.

1. Introduction

1.1. Motivation

As the high penetration of the distributed generation (DG) and flexible loads, the power electronic trend expands in the wide-area transmission network [1,2]. The long-distance transmission lines are geographically dispersed and exposed to the uncertain environment, which leads to the important change in the power system operation [3–5]. Therefore, the wide-area transmission network is easily affected by the various high-impedance surface such as the stone, sand or asphalt [6]. When a fault occurring in the wide-area transmission network, the fault branch isolated by the protection relay and the rest of the grid will be stressed. In the short circuit fault condition, the wide-area transmission network should classify the fault section and self-heal rapidly [7].

1.2. Literature review

The fault classification methods for the wide-area transmission network contain the traveling wave method, the impedance-based method and the intelligent method [8–10].

The traveling wave method computes the fault distance based on the incident reflected traveling wave in the monitoring terminal. Wang [11] concludes that the accuracy of the traveling wave method can be further improved if detail line model is employed. Wide-area traveling-wave methods yield accurate result, while require high sample rate of measurements (MHz) [12]. With the lower sample rate measurement, the impedance methods can estimate fault classification using synchronized signals. The impedance-based method establishes the fault detection equation using the impedance between the fault point and the measuring terminal and detect the fault state. Sano [13] emphasizes that the simplified transmission line model is commonly accepted in the impedance-based method for the transmission network. Aiming at the

* Corresponding authors.

E-mail addresses: zhangtongneuse@163.com (T. Zhang), wanganan0602@163.com (N. Wang).

series compensated transmission line model, Ghazizadeh [14] simplifies the compensation model to derive the nonlinear current distribution matrix and classify the fault phase independent from the measurement type. To guarantee the classification accuracy, Han [15] uses a lumped transmission line model to calculate the capacitor impedance in the valid classification formula. Several model-based methods are summarized and the model accuracy affect the equivalent impedance directly.

Wu [16] concludes that the best global performance method proposes a more suitable model for the transmission line, which allows the consistency correction of the calculated impedance and the nominal one to identify the fault state. Due to the generalization and efficiency, the impedance-based method achieves accurate performance in fault classification for the two-terminal transmission line. The above impedance-based methods concentrate on the amplitude characteristic and the phase angle characteristic requires deeper analysis. Paladhi [17] predicts the sequence current angle characteristic in the fault loop to determine the pure-fault plant impedance for fault type classification. Angela [18] characterizes the phase-angle shift characteristic associated with local voltage sags in uni-directional radial branch and illustrates the basic classification principle as a system impedance function. Therefore, the phase-angle shift character in the single line to ground fault needs further analysis.

To reduce the model dependence effect on the fault classification accuracy, the data-driven intelligent method is introduced to the transmission network. Recent literatures indicate that data-driven fault detection method is efficient to adapt to the transmission system with DGs. Mohammad [19] classifies the system operation state using the variant convolutional neural network, where the voltage amplitude signal is extracted for the regression process. In the regression process, the CNN performance is highly dependent on the mass fault training samples. For each fault type, 12 fault cases are used to train the CNN-based classifier. Shazdeh [20] extracted the current phase angle shift as distinctive features to identify the faulty section. The fault feature accuracy is improved by comparing the phasor shift in the fault process. Bai [21] extracts the fault feature of the partial discharge based on the wavelet analysis. The neural network model predicts the exact output corresponding to the fault area and discriminate from the normal transient operation. Limited by the measurement synchronization [22], few works of fault classification for multi-terminal branches based on the wide-area phase angle analysis are reported. The fault classification method in this paper differs from the existing ones since the phase angle relationship between different geographical positions. The proposed method is robust to the topological structure of network, the type of fault or the DG presence, which improves the accuracy and flexibility.

1.3. Contribution and paper organization

The major contributions of the paper are summarized as follows:

- Spatiotemporal characteristic analysis for the SLG fault process using the hyperbolic tangent model.
- Nonlinear classification is converted into the linear entropy detection based on the characteristic entropy theory.
- The global and local discriminant analysis (GLDA) framework is utilized to restrict the searching range to improve the classification range.

Further, the rest of the paper is organized in five sections. Based on the phasor shift analysis, the fault characteristic model is proposed to extract the signal sag of the fault progress in Section 2. Section 3 implements the characteristic entropy (CE) of the grid impedance to quantify the dispersion of the fault characteristic model and the nonlinear estimation problem is converted into a linear entropy problem. The GLDA-CE fault classification performance is analyzed considering the operating condition, fault situation and measurement noise effect in Section 4. The survey is concluded in Section 5.

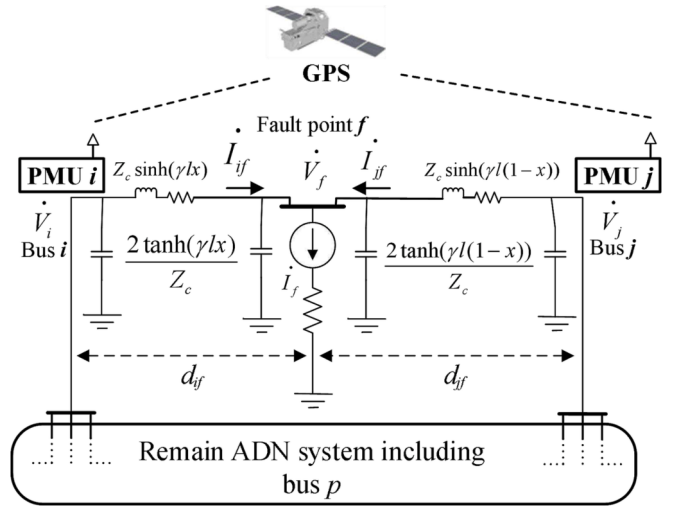


Fig. 1. The circuit model of the long-distance power line in the dynamic SLG fault process using the distribution parameter line model.

2. Local spatial-temporal phasor characterization

Considering a random fault distance in the circuit-analysis derived model, the relationship between the voltage phase angle shift at two arbitrary points of long-distance transmission line can be estimated. By phase analysis in the dynamic process, the phasor shift relation between voltage and current angles is used to characterize the synchronization signal sags in the fault position. The nonlinear characteristic model for the active power flow in a transmission branch is established by stages, which is described by the hyperbolic tangent function. Since the characteristic model is nonlinear and identified by the entropy index to measure the characteristic matrix consistency.

2.1. Spatiotemporal characteristic analysis of the adjacent current

To illustrate the basic principle of the impedance classification method, an equivalent circuit model of the medium-length transmission line is illustrated in Fig. 1. Considering a single line to ground (SLG) fault at fault position f along the random transmission line $i-j$, the fault point divides the line section into two segments, which is modeled by the distributed parameter line model.

Voltage at random point is predicted based on an equivalent electrical circuit of line lump with concentrated parameters in Fig. 1. The transfer impedance vector Z_{kf} of the monitoring PMU sensor in the long-distance power line considering the distributed parameter line model. When the multi-concurrent fault occurs in the n -bus system, the fault point f is updated as a new virtual bus $n+1$ and the resistance matrix is extended as $Z_e = [Z_{k,1}, Z_{k,2} \dots Z_{k,n}, Z_{k,n}(d_f); Z_{n+1,1}, Z_{n+1,2} \dots Z_{n+1,n}, Z_{n+1,n+1}(d_f)]$, ($k = 1, 2, \dots, n$). Calculated from the upstream i_{th} bus, the injection current $I_{i,n}$ from bus I is predicted with the two port network form using the boundary condition as

$$I_{i,n} = \sinh(\gamma_{ij} d_f) U_i / Z_c + Z_c \cosh(\gamma_{ij} d_f) I_i \quad (1)$$

The current I_j at the downstream j_{th} bus from p_{th} bus is

$$\begin{aligned} I_j &= (I_p Z_{j,p} \cosh(\gamma_{ij}(l - d_f)) - I_i Z_c \sinh(\gamma_{ij} d_f)) \frac{n!}{r!(n-r)!} \\ &\quad - I_p Z_{i,p} \cosh(\gamma_{ij} d_f) / Z_c \sinh(\gamma_{ij}(l - d_f)) \end{aligned} \quad (2)$$

The downstream current I_{n+1} from the line terminal meets Kirchhoff current law as

$$I_{i,n} = \sinh(\gamma_{ij} d_f) U_i / Z_c + Z_c \cosh(\gamma_{ij} d_f) I_i \quad (3)$$

The injection current $I_{j,n+1}$ from j_{th} terminal is predicted as

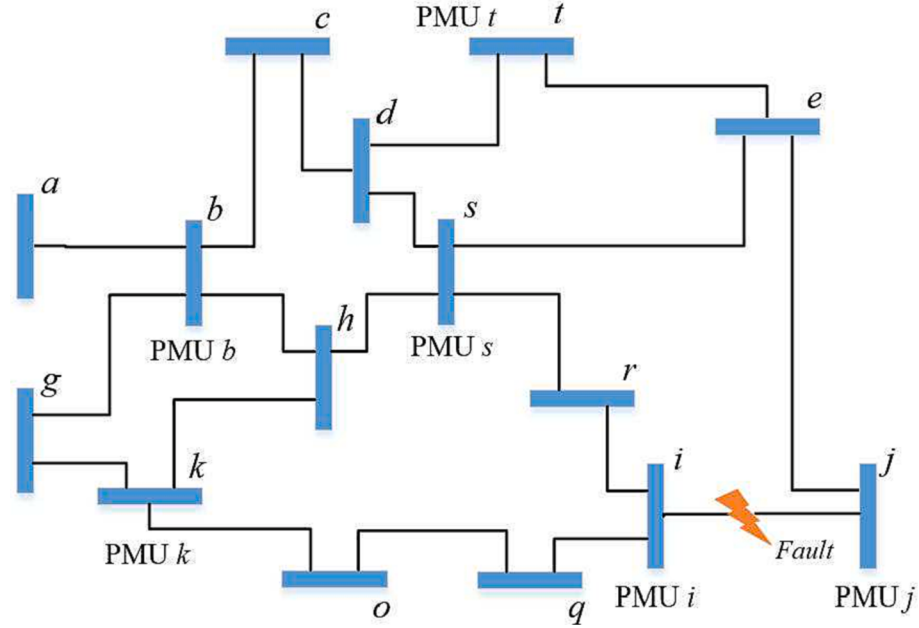


Fig. 2. The PMU sensor installation schematic diagram.

$$I_{j,n+1} = \sinh(\gamma_{ij}(l - d_f))U_j/Z_c + Z_c \cosh(\gamma_{ij}(l - d_f))I_j \quad (4)$$

Considering the fault injection current $I_{i,n+1}$ and $I_{j,n+1}$ from terminal i and j , the fault current I_{n+1} can be predicted from p_{th} bus as

$$I_{n+1} = I_p Z_{i,p} \cosh(\gamma_{ij} l) / Z_c \sinh(\gamma_{ij} (l - d_f)) - I_p Z_{j,p} / Z_c \sinh(\gamma_{ij} (l - d_f)) + I_i Z_c \sinh(\gamma_{ij} l) / Z_c \sinh(\gamma_{ij} (l - d_f)) \quad (5)$$

Based on the mutual impedance, the transfer impedance vector $Z_{p,n+1}$ between the p_{th} bus and fault point f is

$$\begin{aligned} Z_{k,n+1} &= (Z_{k,i}(Z_{n+1}Z_{jk}\sinh(\gamma_{ij}d_f) + Z_c^2Z_{i,k}\cosh(\gamma_{ij}d_f)^2\sinh(\gamma_{ij}l)) \\ &- Z_jZ_{i,k}\sinh(\gamma_{ij}d_f)\cosh(\gamma_{ij}l) - Z_c^2Z_{i,k}\cosh(\gamma_{ij}d_f)\sinh(\gamma_{ij}d_f) \\ &\cosh(\gamma_{ij}l)) / Z_{i,k}Z_c\cosh(\gamma_{ij}l) - Z_cZ_{j,k} + Z_c^2Z_{i,k}\cosh(\gamma_{ij}d_f)\sinh(\gamma_{ij}l)) \end{aligned} \quad (6)$$

Considering the metallic short circuit fault effect, the boundary condition of the two port network in Eq. (1) is extended. Therefore the discrete state space of the voltage sag ΔU at random bus in the initial fault process is

$$\begin{bmatrix} U_p(t+1) - U_p(t) \\ U_{n+1}(t+1) - U_{n+1}(t) \end{bmatrix} = Z_e \begin{bmatrix} 0 \\ I_{n+1}(t+1) \end{bmatrix} \quad (7)$$

where $U_p(t)$ is the health state voltage at p_{th} bus, $U_p(t+1)$ is the fault progress voltage at p_{th} bus. Therefore, the fault current $I_{n+1}(t+1)$ is

$$I_{n+1}(t+1) = \Delta U_i(t+1) / Z_{i,n+1}(d_f) \quad (8)$$

In the metallic short circuit fault scenario, the transfer impedance at the extended virtual bus shows the pure resistance. From the monitoring bus i and j , the phase shift in the fault branch satisfies

$$\arg(U_{n+1}(t+1)) = \arg(I_{n+1}(t+1)) \quad (9)$$

2.2. Characteristic entropy

The nonlinear characteristic model extracts the non-stationary fault characteristic using PMU sensor. In view of the thermodynamics entropy, information entropy was propounded to evaluate the system consistency [23–25]. Entropy has the following properties:

The entropy method quantifies the pattern similarity degree in the time series and measures the signal consistency, which is robust to measurement noise and shows well tolerance for the transient interference;

The entropy method describes the sequence complexity statistically instead of describing and reconstructing the whole signal sequence. The limited data can calculate the reasonable and robust estimation.

The entropy relies on the probability distribution rather than the amplitude and is related to higher order moments [26–28], which can offer a better nonlinear characterization of the system consistency. Therefore based on the Shannon entropy theory, the CE classification method measures the consistency of the nonlinear fault characteristic model. The nonlinear fault classification problem for the long-distance power line is converted into the linear entropy problem.

In the fault detection state, the synchronized current phase signal is measured by PMU sensors at p_{th} bus and the time-series phase characteristic φ_p satisfies

$$e^{i\varphi_p}(t+1) = \Delta U_p(t+1) / (Z_{p,n+1}(d_f)I_p(t+1)) \quad (10)$$

Generated to the wide-area transmission network, the fault character matrix is normalized as $\Lambda = [\lambda_1, \lambda_2 \dots \lambda_p]$ ($\lambda_p = [\lambda_{n,1}, \lambda_{n,2} \dots \lambda_{n,p}]$).

$$\lambda_p(t+1) = \varphi_p(t+1) / \max_n \{\varphi_{1,p}(t+1), \varphi_{2,p}(t+1), \dots, \varphi_{n,p}(t+1)\} \quad (11)$$

The discrete entropy characteristic $e(t+1)$ at p_{th} bus from fault point f is

$$e_{p,n+1}(t+1) = -\lambda_{p,n+1}(t+1) \ln(\lambda_{p,n+1}(t+1)) \quad (12)$$

The discrete entropy characteristic $e(t+1)$ quantifies the characteristic consistency. The ordered system contains the lower entropy. When the probability mass concentrates at a single point, the entropy minimum value in the Dirac delta distribution. Then, the fault phase is identified as the minimum entropy $e(t+1, d_f)$. Based on the minimum search, the GLDA-CE method can identify the fault phase quantitatively and directly, which simplifies the training process of the artificial intelligence algorithms.

3. Multi-priority GLDA-CE fault classification framework

The distributed fault classification strategy contains two stages. First, in the wide area PMU monitor system, the potential fault section is estimated based on the detection criteria. Then, in the potential fault terminal, the voltage and current phase signals are predicted and the fault phase is identified based on the classification criteria.

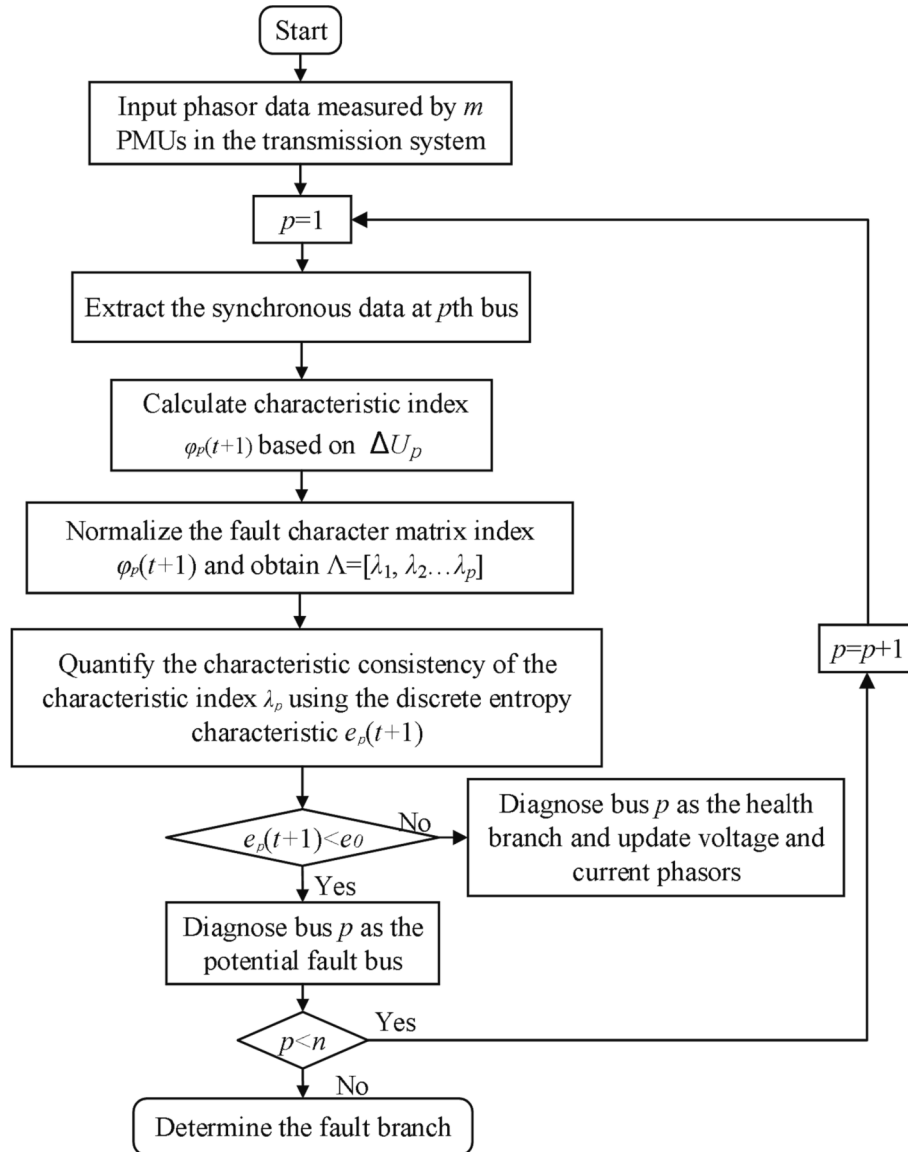


Fig. 3. Flowchart for global clustering fault detection.

3.1. Global clustering probability for fault detection

In the wide area transmission network, the fault detection time is long through analyzing operating state of each bus. As a result, the fault detection time decreases through the fault section estimation and reducing searching region.

Assuming that the PMU sensors are installed at bus b, i, j, k, s, t and a metal fault occurs at bus f in Fig. 2. The discrete entropy value $e(t+1, d_f)$ of the fault characteristic value at bus i and j decreases. In the dynamic fault process, the phase characteristic value λ_j nearby the fault point f decreases. In the fault detection stage, the detection criteria identifies the fault bus based on the entropy characteristic. In the wide-area transmission network, phasor characteristic vector $E(t+1)$ ($E(t+1) = [e_1(t+1), e_2(t+1)...e_n(t+1)]$) is

$$E(t+1) = - \sum_{l=1}^m \lambda_l(t+1) \ln \lambda_l(t+1) / \ln(n) \quad (13)$$

Then the discrete entropy characteristic vector $E_p(t+1)$ at p_{th} bus is sorted and the phase order degree is quantified to identify the fault section. The fault detection criteria identifies the fault bus i^* as

$$i^* \in \min_n \{e_n(t+1)\} \quad (14)$$

In the actual long-distance power line, the fault may happen in the multi-terminal transmission branches. The fault characteristic $E_p(t+1)$ at p_{th} suspicious branches connected to bus p are calculated to estimate the fault branch. Then, the $i-j$ fault branch is diagnosed as the minimum characteristic entropy in Fig. 3.

3.2. Distributed fault classification criteria

The potential fault branch obtains the higher priority of the classification research based on the above fault detection result. The PMU sensors track the voltage phasors form the two terminals of the potential fault branch $i-j$. The phase angle relationship between the phase angle of the fault current can be expressed in hyperbolic tangent functions and $\varphi_{p,i}$ is calculated as

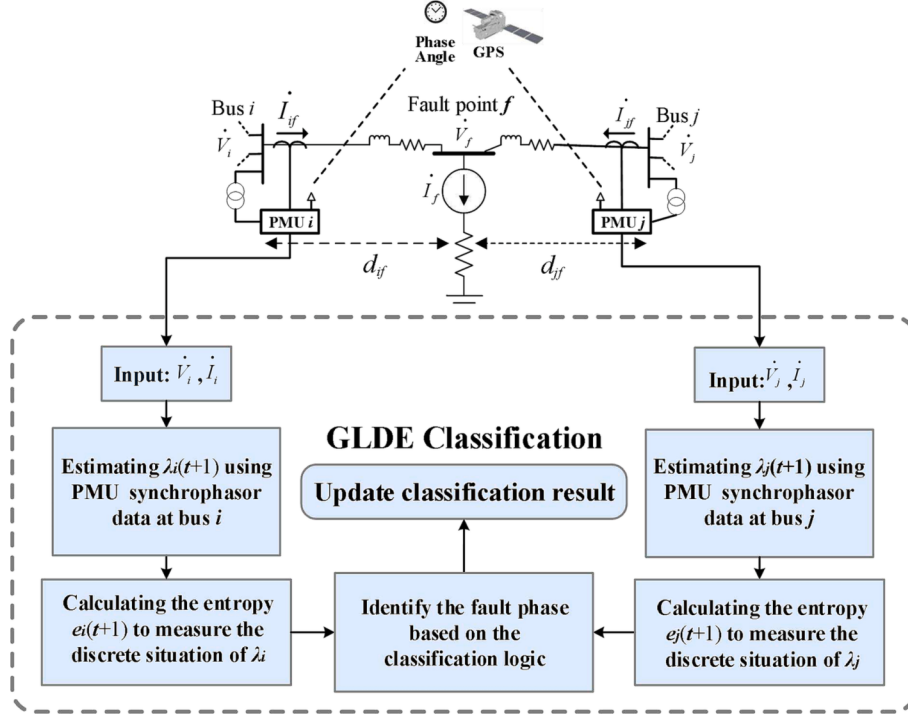


Fig. 4. Schematic diagram for the GLDA-CE fault classification method.

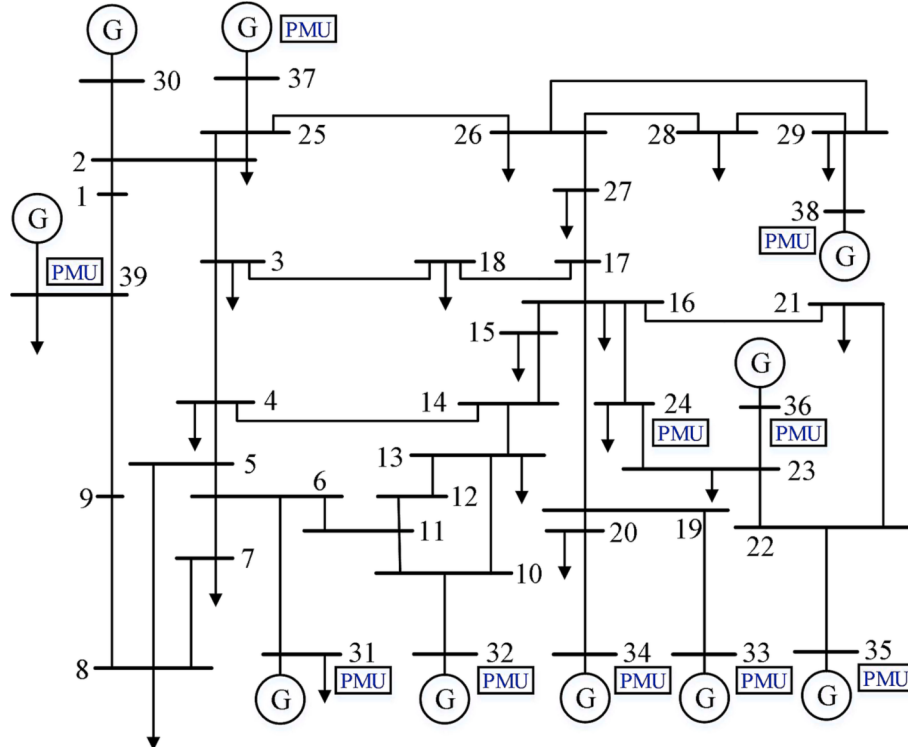


Fig. 5. The IEEE 39-bus test medium-scale transmission network WITH 10 PMUs.

$$\begin{aligned} \varphi_{p,i}(d_f, t+1) = & \arg((\Delta U_p(t+1)(Z_c \cosh(\gamma_{ij} l) - Z_c^2 Z_{p,i} \cosh(\gamma_{ij} d_f)) \\ & \sinh(\gamma_{ij})) / (Z_{i,p}(Z_{n+1} \sinh(\gamma_{ij} d_f) + Z_c^2 Z_{p,i} \cosh(\gamma_{ij} d_f)^2) \\ & \sinh(\gamma_{ij}) - Z_{n+1} \sinh(\gamma_{ij} d_f) \cosh(\gamma_{ij} l) - Z_c^2 \cosh(\gamma_{ij} d_f) \sinh(\gamma_{ij} l))) \end{aligned} \quad (15)$$

The discriminant logic of the fault classification model is

$$(C_p^F(t), T_F^C) = (\{(i, p, T_s) | \lambda_{p,i}(t, d_f) \leq \delta^p\}) \quad (16)$$

where T_F^C is the respond time, i is the PMU monitoring bus, $C_p^F(t)$ is the health state of p_{th} bus at time t . In the health state, $C_p^F = \emptyset$. In the fault state, $C_p^F \in [1 \dots n]$.

In Eq. (16), the denominator order is much higher than the

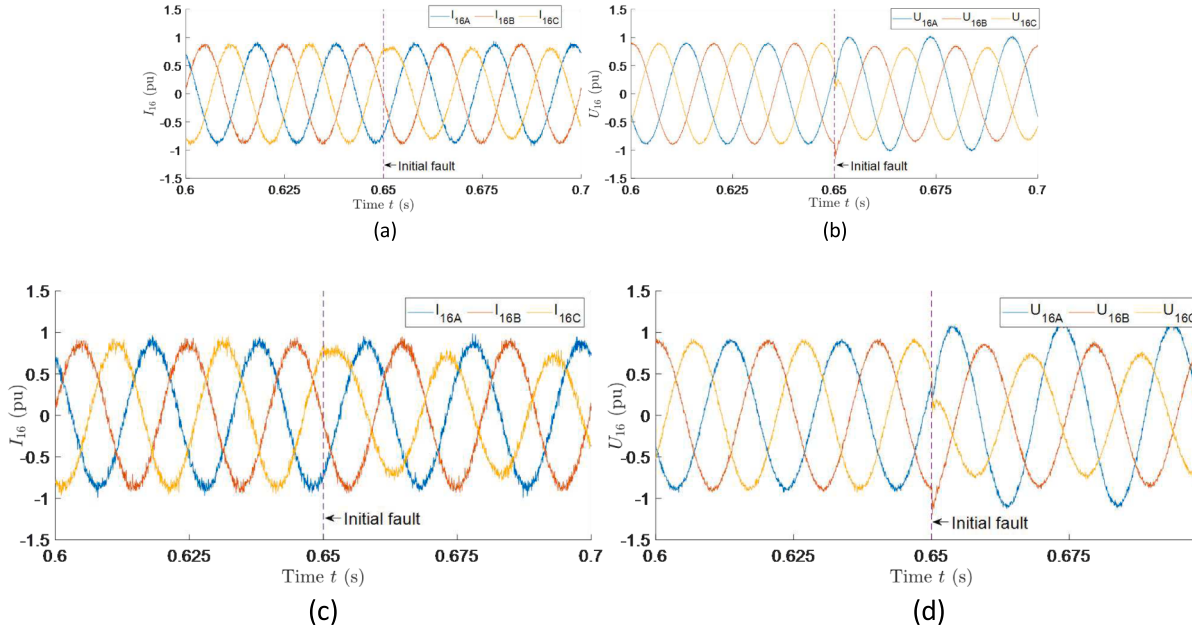


Fig. 6. The pre- and post-fault waveforms of synchronized voltage and current at bus 16 and fault occurs on phase C at 0.65 s: (a) I_{16} at 35 dB level; (b) U_{16} at 35 dB level; (c) I_{16} at 30 dB level; (b) U_{16} at 30 dB level.

numerator order. Therefore, the Z_{n+1} increases to the threshold value, the $\arg(\Delta U_p/Z_{n+1})$ remains to the constant. This work constructs a fault characteristic model based on the fault angle analysis. The fault resistance has weak influence on the GLDA-CE classification accuracy.

Instead of analyzing the operating state at each bus, the GLDA-CE fault classification method first estimates the fault branch based on the spatiotemporal characteristic analysis to reduce the observation space dimension. Then GLDA-CE fault classification method measures the spatiotemporal order degree using the local PMU-measured data to identify the fault phase. Thus, in the wide area transmission and transmission network, the multi-priority fault classification strategy can achieve second-level response in Fig. 4.

4. Results and discussion

4.1. Characteristic extraction in time domain

To verify the efficiency of GLDA-CE fault classification method, the fault detection tests are operated in the 12.66-kV IEEE 39-bus system [29–31] includes 39 buses, 43 branches, and 10 DGs. The PMU sensors installed position based on the observer criteria [32,33] is shown in Fig. 5: 24, 31, 32, 33, 34, 35, 36, 37, 38, 39 bus.

The characteristic extraction is analyzed in the SLG fault scenario. Supposing that a C-phase to ground fault occurs at 82.530% from bus 16 ($i = 16, j = 24, d_f = 0.8253$) in branch 16–24 bus. The transient fault occurs at 0.65 s and is cleared at the 0.66 s. The transmission branch of 16–24 bus is modeled with a total line length of 10 km, the load demand of 15.43 MVA and fault resistance $Z_{n+1} = 30 \Omega$.

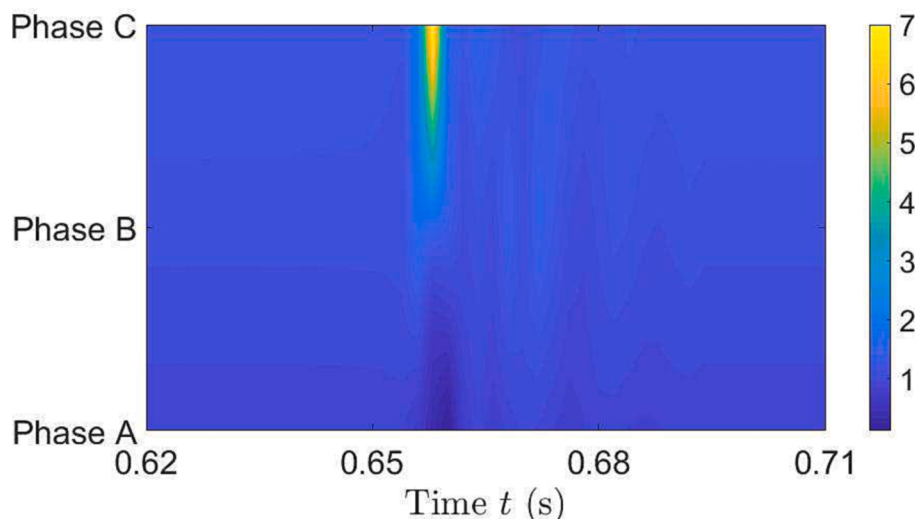


Fig. 7. The fault characteristic component φ_{16} .

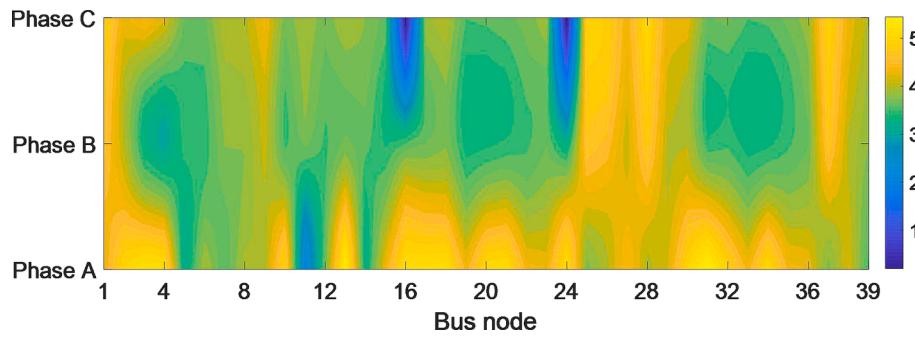


Fig. 8. Fault detection result for the SLG fault in the medium-scale transmission network.

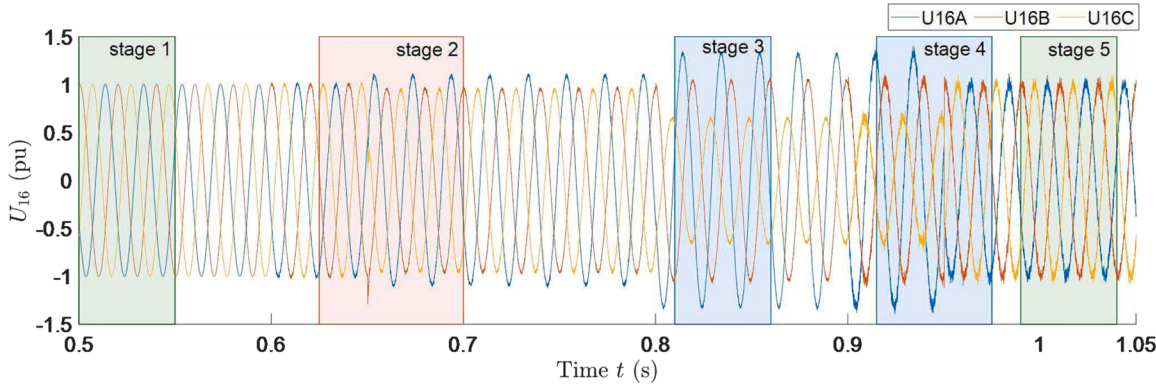


Fig. 9. The PMU-measured voltage U_{16A} , U_{16B} , U_{16C} in the SLG fault process in the noise scenario ($\text{SINR} = 20 \text{ dB}, 30 \text{ dB}$).

4.1.1. Evolution of real-time power amplitude in time domain

In the IEEE-39 power system, an C-phase to ground fault occurs in the 16–24 branch. The voltage and current signals are analyzed at different measurement noise level in Fig. 6. The voltage and current signals of bus 24 containing white Gaussian noise, where $\text{SNR} = 30 \text{ dB}$ and 35 dB in the dynamic fault progress. In Fig. 6(a), the 35 dB noise signal affects the magnitude of current and voltage at 1.861% . In Fig. 6(b) the 30 dB noise signal affect the magnitude at 4.352% .

4.1.2. Spatiotemporal characteristic analysis of the adjacent current

The fault characteristic φ_{16} in the 16–24 branch is shown in Fig. 7. In the normal operation progress (0 – 0.65 s), the φ_{16c} remains at 1.290 . In the fault initial stage, the fault characteristic φ_{24c} increase to 7.031 within 0.04 s while φ_{16A} and φ_{16B} maintain the normal state ($\varphi_{16A} = 1.599$ and $\varphi_{16B} = 0.741$). In the high-resistance fault scenario, the current magnitude signal of the fault transmission branch changes slightly 1.893% . The fault current flow direction in the fault branch changes more significantly, which is measured by the characteristic signals of the phased angle. Based on phase angle analysis, the proposed characteristic model can extract the transient sag and represent the dynamic behavior of the high-resistance fault in the power line.

4.2. Spatiotemporal analysis of fault classification

4.2.1. Global global inter-domain fault detection

To verify the detection efficiency, based on the detection criteria, the CE vector e_i for the transmission network is calculated in Fig. 8. In Fig. 8, e_{16} is 0.242 and e_{24} is 0.203 , which detects a fault in branch 16–24. The characteristic entropy e_{16} and e_{24} decrease significantly comparing with the nearby buses, which corresponds to that only the characteristic vector of the fault branch is well ordered while the normal bus is disorder.

4.2.2. Analysis of fault classification at different SNR level

In the SLG fault scenario of Fig. 7, the corresponding detection result r_{24} is analyzed in Figs. 9 and 10. In Fig. 10(a) (stage 1), the residual confidence interval $e_{16c} = [0.005, 0.018]$ in the normal state. In stage 2, a SLG fault occurs in phase C (branch 16–24) at 0.65 s ($\text{SINR} = 20 \text{ dB}$) and $e_{16c} = [0.057, 0.083]$ with the confidence level 99.00% . In stage 4, the restoration relay acts at 0.95 s ($\text{SINR} = 30 \text{ dB}$) and $e_{16c} = [1.218, 1.374]$ with the confidence level 97.323% and the response time $t_{CE} = 0.02 \text{ s}$.

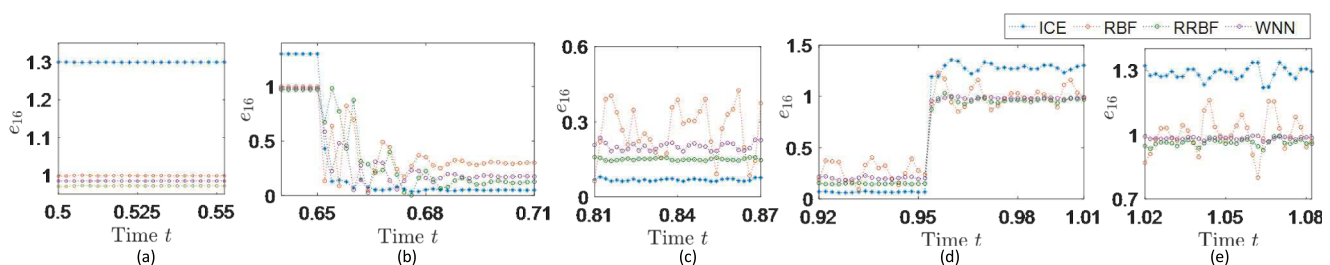


Fig. 10. Dynamic detection result e_{16} : (a) e_{16} in stage 1; (b) stage 2; (c) stage 3; (d) stage 4; (e) stage 5.

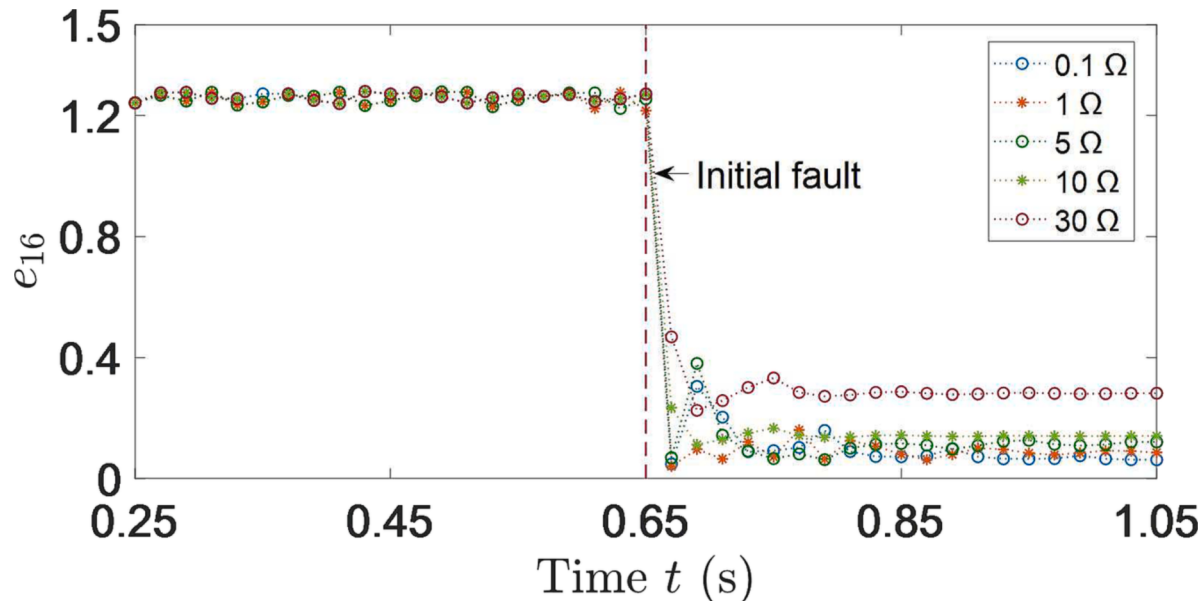


Fig. 11. GLDA-CE detection result e_{16} in the long-distance power line at different transition resistance.

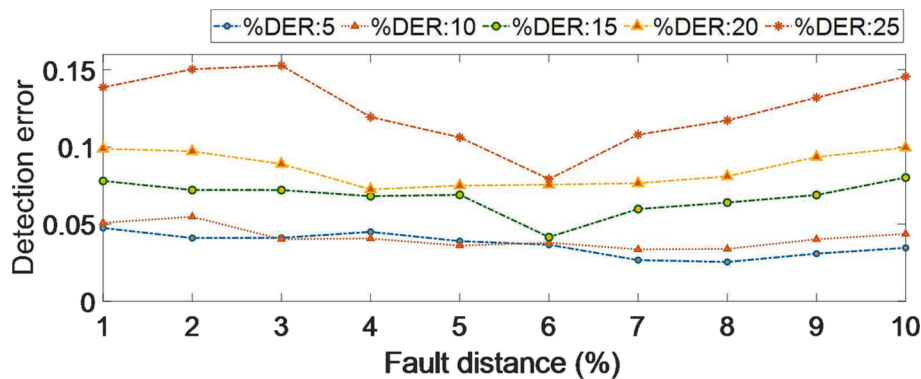


Fig. 12. Detection performance of the proposed GLDA-CE method at increasing DG penetration level.

4.2.3. Composition analysis at different transition resistance

Assuming that a C-phase to ground fault occurs at the 20% distance from bus 24 in the 16–24 branch; the fault occurs at 1 s and is cleared at 3 s; fault resistance Z_{n+1} range [0.1, 30].

The synchronized detection result at bus 16 in the dynamic fault process is shown in Fig. 11. In the health state, the CE curves e_{16} maintain to 1.252 and fluctuate slightly. At the fault initial process, the CE curves e_{16} decreases 94.449% in 0.65 s.

In Fig. 11, the entropy $e_{16-0.1}$ drops to 0.048 in 0.02 s ($Z_{n+1} = 0.1 \Omega$); e_{16-1} drops to 0.062 in 0.12 s ($Z_{n+1} = 1 \Omega$); e_{16-5} drops to 0.091 in 0.16 s ($Z_{n+1} = 5 \Omega$); e_{16-10} drops to 0.146 in 0.20 s ($Z_{n+1} = 10 \Omega$); e_{16-30} drops to 0.313 in 0.24 s ($Z_{n+1} = 30 \Omega$). The characteristic entropy e_{16} increases slightly as the fault resistance increases, which below the threshold 0.6. In the 600 test cases, the detection accuracy is 99.667% and the respond time is within 0.1 s.

In order to test the effect of DG penetration level, five groups of simulation tests are conducted in 16–24 branch. The detection errors of the proposed GLDA-CE fault classification method are shown with the increasing DG penetration level in Fig. 12. For this case, the proposed GLDA-CE method exhibits an increasing detection error trend as the DG penetration level increases, reaching an average error of 0.0412 for a penetration level of 25%. This behavior is due to the increasing penetration, which increases the error of voltage signal U_{16} contributed to the training sets of the transmission systems.

Table 1

Classification false alarm rate r by applying four different methods to three data sets.

Transition impedance	$r_{\text{GLDA-CE}} \%$	$r_{\text{INNC}} \%$	$r_{\text{RRBF}} \%$	$r_{\text{WNN}} \%$
0.1 Ω	0.923	1.154	3.846	5.769
10 Ω	1.462	4.846	15.385	17.077
30 Ω	1.769	5.385	16.231	17.308

Based on the detection criteria, the characteristic-based method analyzes the consistency of fault characteristics, which is independent of the magnitude signal. The GLDA-CE detection method can monitor the wide-area power system synchronously in both low resistance and high resistance fault process.

4.2.4. Computational effectiveness analysis

To analyze the method sensitivity, the fault resistance effect on the path of grounding oscillatory circuit is considered. In Table 1, the classification accuracy and respond time evaluate the classification performance of the GLDA-CE classification method comparing with the nearest neighbor clustering (NNC) method [34], regularized radial basis neural network (RRBF) [35] and wavelet neural network (WNN) [36] method. The average classification false alarm rate $r_{\text{GLDA-CE}}$ is 1.385%, which decreases 2.411% of r_{INNC} . Meanwhile, the classification false

Table 2Respond time t by applying four different methods to three data sets.

Transition impedance	$t_{\text{GLDA-CE}}$ s	t_{INNC} s	t_{RRBF} s	t_{WNN} s
Health state	0.857	5.865	51.319	24.584
10 Ω	1.343	5.287	55.088	25.210
30 Ω	1.621	6.254	57.507	38.135

alarm rate of the artificial neural network (ANN) methods are much higher ($r_{\text{RRBF}} = 11.821\%$, $r_{\text{WNN}} = 13.385\%$), which leads to misjudgments. Therefore, the GLDA-CE classification method shows the lowest classification error.

In Table 2, the response time t of the GLDA-CE, INNC, RRBF and WNN method are compared. Due to the proposed method extracts the fault characteristic from the ADN system essentially and identify the fault phase based on the classification model synchronously, the GLDA-CE respond time $t_{\text{GLDA-CE}}$ is 1.273 s, which is far below the ANN methods. Different from the ANN methods, the GLDA-CE method is independent from the complex calculation and training process. In the impedance method, the classification accuracy depends on the iterations of the matching degree and affects the classification response time directly. Therefore, the proposed GLDA-CE classification method can extract the fault characteristic from measurement noise interference clearly and improves the search efficiency.

5. Conclusion

A novel fault classification method based on the spatiotemporal characteristic analysis for the wide-area transmission network is proposed in this paper. The transient spatiotemporal characteristic of the fault current is extracted in the dynamic progress. The fault classification criteria quantifies the order degree of the spatiotemporal characteristic. The characteristic enhancement and the coordinating identification framework confirm that the GLDA-CE fault classification method obtains the high generalization capability in the measurement noise and fault resistance effect. The hierarchical classification strategy reduces the fault search zone and decreases the respond time. Therefore, the GLDA-CE fault classification method obtains the classification accuracy 92.414% and the fast respond time 1.274 s compared with the WNN, RRBF and INNC method. The GLDA-CE fault classification method can monitor the power system synchronously and lays the foundation for the transmission system restoration.

Declaration of Competing Interest

The authors declare that they have no known competing financial interests or personal relationships that could have appeared to influence the work reported in this paper.

Acknowledgments

This work is financially supported by Cultivation Foundation of Shenyang University of Technology (No. 200005848), China Postdoctoral Science Foundation (2021 M700093), Natural Science Foundation Project of Liaoning Province (No. 2023-BS-206), National Natural Foundation of China (No. 51775094) and Liaoning Province Applied Basic Research Program (No. 2023JH2/101300237).

References

- [1] N. Gupta, K. Seethalekshmi, S.S. Datta, Wavelet based real-time monitoring of electrical signals in Distributed Generation (DG) integrated system, Eng. Sci. Technol. 24 (2021) 218–228.
- [2] A.A. Sadiq, S.S. Adamu, M. Buhari, Optimal distributed generation planning in distribution networks: A comparison of transmission network models with FACTS, Eng. Sci. Technol. 22 (2019) 33–46.
- [3] B. Taheri, S. Salehimehr, M. Sedighizadeh, Fault-location algorithm for parallel line based on the long short-term memory model using the distributed parameter line model, Int. J. Elec. Power. 31 (2021) 13032.
- [4] Y.P. Ma, Q.W. Li, L.L. Chu, Real-time detection and spatial localization of insulators for UAV inspection based on binocular stereo vision, Remote Sens. 13 (2021) 230.
- [5] V. Psaras, D. Tzelepis, G. Burt, HVDC grid fault location method using genetic algorithm on reconstructed frequency-domain voltage profiles, Int. J. Elec. Power. 144 (2023) 1–8.
- [6] S. Belagoune, N. Bali, A. Bakdi, Deep learning through LSTM classification and regression for power line fault detection, detection and location in large-scale multi-machine power systems, Measurement 177 (2019), 109330.
- [7] X. Xiong, W. Yao, W. Chen, A data-driven approach for fault time determination and fault area location using random matrix theory, Int. J. Elec. Power. 116 (2020), 105566.
- [8] X. Jin, X.Y. Chen, C. Qi, T. Li, Investigation on the electromagnetic surface waves for single-wire power transmission, IEEE Trans. Ind. Electron. 70 (2023) 2497–2507.
- [9] S. Kiranyaz, O. Avci, O. Abdeljaber, 1D convolutional neural networks and applications: A survey, Mech. Syst. Signal Pr. 151 (2021) 1–21.
- [10] P. Stefanidou-Vozikli, N. Sapountzoglou, B. Raison, A review of fault location and classification methods in distribution grids, Electr. Pow. Syst. Res. 209 (2022) 1–8.
- [11] H.Z. Wang, X.Z. Dong, Traveling wave based differential protection for renewable energy penetrated power system, J. Electr. Eng. Technol. 17 (2022) 1623–1630.
- [12] Z.J. Liu, X. Hu, T. Liu, Predistortion with low feedback sampling rate for wideband nonlinear satellite downlinks, IEEE Commun Lett. 23 (2019) 2367–2371.
- [13] K. Sano, S. Horiuchi, T. Noda, Comparison and selection of grid-tied inverter models for accurate and efficient EMT simulations, IEEE Trans. Power Electr. 37 (2022) 3462–3472.
- [14] M. Ghazizadeh, Time-domain based fault location for series compensated power lines without retriggering fault type, Electr. Pow. Syst. Res. 181 (2020), 106171.
- [15] J. Han, S.H. Miao, Y.W. Li, Faulted-Phase classification for power lines using gradient similarity visualization and cross-domain adaption-based convolutional neural network, Electr Pow Syst Res. 191 (2021), 106876.
- [16] S.P. Wu, J. Fan, Modeling of crosstalk between two nonparallel striplines on adjacent layers, IEEE Trans. Electromagn. C. 55 (2014) 1302–1310.
- [17] S. Paladhi, A.K. Pradhan, Adaptive fault type classification for transmission network connecting converter-integrated renewable plants, IEEE Syst J. 15 (2021) 4025–4036.
- [18] A. Espin, J.R. Camarillo, G. Ramos, Characterization of phase-angle jump in radial systems using incremental voltage phasors, IEEE Trans. Ind. Appl. 55 (2019) 1117–1125.
- [19] M. Alqudah, M. Pavloski, T. Dokic, Fault detection utilizing convolution neural network on timeseries synchrophasor data from phasor measurement units, IEEE Trans. Power Syst. 37 (2022) 3434–3442.
- [20] S. Shazdeh, H. Golpira, H. Bevrani, A PMU-based back-up protection scheme for fault detection considering uncertainties, Int. J. Elec. Power. 145 (2023) 1–11.
- [21] F.F. Bai, Y. Cui, R.F. Yan, Cost-effective synchrophasor data source authentication based on multiscale adaptive coupling correlation detrended analysis, Int. J. Elec. Power. 144 (2023) 1–8.
- [22] A. Arunkumar, N. Gupta, A. Pinceti, PMUVIS: a large-scale platform to assist power system operators in a smart grid, IEEE Comput. Graph. 42 (2023) 84–95.
- [23] A.R. Abbasi, C.P. Gandhi, A novel hyperbolic fuzzy entropy measure for discrimination and taxonomy of transformer winding faults, IEEE Trans. Instrum. Meas. 71 (2022) 1–8.
- [24] J.L. Sun, L.D. Geng, Y.Z. Wang, A hybrid model based on superpixel entropy discrimination for PolSAR image classification, Remote Sens. 14 (2022) 4116.
- [25] Z. Zhang, D.G. Wang, X. Sun, Spatial sampling and grouping information entropy strategy based on kernel fuzzy C-means clustering method for hyperspectral band selection, Remote Sens. 14 (2022) 5058.
- [26] D.L. Mu, S. Lin, H.Q. Zhang, Novel fault identification method for HVDC converter station section based on energy relative entropy, IEEE Trans. Instrum. Meas. 71 (2022).
- [27] D.L. Mu, S. Lin, H.Q. Zhang, T. Zheng, A novel fault identification method for HVDC converter station section based on energy relative entropy, IEEE Trans. Instrum. Meas. 71 (2022), 3507910.
- [28] C.Y. Ma, Y.B. Li, X.Z. Wang, Z.Q. Cai, Early fault diagnosis of rotating machinery based on composite zoom permutation entropy, Reliab. Eng. Syst. Safe. 230 (2022), 108967.
- [29] C. Zhang, M.M. Zhang, Wavelet-based neural network with genetic algorithm optimization for generation prediction of PV plants, Energy Rep. 8 (2022) 10976–10990.
- [30] Z.S. Chafi, H. Afrakhte, Wide area fault location on transmission networks using synchronized/unsynchronized voltage/current measurements, Electr. Pow. Syst. Res. 197 (2021), 107285.
- [31] Y.S. Bai, S.Y. Li, X.P. Gu, G.Q. Zhou, Collaborative planning of resilient backbone grids and PMU placement for power systems, Int. J. Elec. Power. 131 (2021), 107106.
- [32] G. Pierrou, X.Z. Wang, An Online Network Model-Free Wide-Area Voltage Control Method Using PMUs, IEEE T Power Syst. 36 (2021) 4672–4682.
- [33] T. Zhang, H.B. Yu, J.C. Liu, Single phase fault detection and location in active distribution network using synchronized voltage measurement, Int. J. Elec. Power. 117 (2020), 105572.

- [34] S. Zhang, H. Chen, J. Tang, Fault location based on voltage measurement at secondary side of low-voltage transformer in distribution network, *IEEE Trans. Instrum. Meas.* 71 (2022) 3522512.
- [35] H. Ehyi, T.N. Skreien, A. Nysveen, Intelligent data-driven diagnosis of incipient interturn short circuit fault in field winding of salient pole synchronous generators, *IEEE T Ind Inform.* 18 (2022) 3286–3294.
- [36] E. Tsotsopoulou, X. Karagiannis, P. Papadopoulos, Time-domain protection of superconducting cables based on artificial intelligence classifiers, *IEEE Access.* 10 (2022) 10124–10138.